TECHNICAL TRANSACTIONS | CZASOPISMO TECHNICZNE
MECHANICS | MECHANIKA
1-M/2016

GEORG BRÖSIGKE, JENS-UWE REPKE*, ALEXANDER HERTER,
MATTHIAS RÄDLE**

ANALYSIS OF THE INFLUENCE OF TURBULENCE ON THE HEAT TRANSFER BETWEEN SPHERICAL PARTICLES AND PLANAR SURFACES

ANALIZA WPŁYWU TURBULENCJI NA TRANSFER CIEPŁA POMIĘDZY CZĄSTKAMI KULISTYMI A PŁASKIMI POWIERZCHNIAMI

Abstract

The heat transfer between particles and walls plays an important role in several industrial processes. Since established models often deal with simplifications for the surrounding gaseous phase, this work aims to acquire a fundamental understanding of the occurring transport phenomena. In this work, a high-resolved finite-volume method is applied carrying out direct numerical simulation of fluid dynamics and heat transfer simultaneously. The influence of turbulence on the heat transfer is discussed in this paper.

Keywords: heat transfer, particles, direct numerical simulation, turbulence

Streszczenie

Przekazywanie ciepła pomiędzy cząstkami i ścianami odgrywa ważną rolę w wielu procesach przemysłowych. W uznanych modelach często wprowadzane są uproszczenia – celem tej pracy był opis fundamentalnych zjawisk transportu. Zastosowano metodę objętości skończonych do przeprowadzenie bezpośredniej symulacji numerycznej ruchu płynu i wymiany ciepła jednocześnie z uwzględnieniem wpływu turbulencji na transfer ciepła.

Słowa kluczowe: przenikanie ciepła, cząstki, symulacja numeryczna bezpośrednia, turbulencja

DOI:

* MSc. Eng. Georg Brösigke, Prof. PhD. DSc. Eng. Jens-Uwe Repke, Process Dynamics and Operations Group, Faculty Of Process Sciences, Technical University of Berlin.
** MSc. Alexander Herter, Prof. PhD. DSc. Matthias Rädle, Hochschule Mannheim.

1. Introduction

The heat transfer between spherical particles and walls on the one hand, and solely between particles on the other hand is relevant in several pieces of industrial apparatus – amongst others, these include fixed-bed reactors, fluidised beds, tube dryers and rotary kilns. The occurring mechanisms are not yet fully understood or rather, their different degrees of contribution have not yet been quantified satisfactorily. For the purposive development and efficient design of the mentioned pieces of apparatus, a fundamental understanding of the occurring mechanisms is crucial.

In previous work [1], the heat conduction through the gaseous gap between a single spherical particle and a planar surface was identified as the dominating mechanism for the laminar regime. The investigation was carried out with CFD simulations and the results were validated against both experimental data and a correlation from literature for a static sphere on a planar surface [2].

For calculating the heat transfer, simplified approaches via Nusselt correlations are often chosen. These correlations frequently neglect transport resistances in the solid phase and the actual fluid dynamics in the surrounding fluid (i.e. gas or liquid) phase.

In order to identify the basic transport mechanisms, the generic system is transformed to a system of basic geometries, i.e. sphere and plate.

2. Methods

Since the particles are small (< 1 mm) an experimental approach would require enormous effort, if it was possible at all; therefore, a 3D finite volume approach was chosen for the simulations in order to resolve both temperature and velocity boundary layers in all involved phases.

2.1. Solver-development

The open source toolbox OpenFOAM® developed on the basis of [3] and [4] was used to carry out the simulations. The toolbox offers a variety of preassembled standard solvers, which can be customised in order to meet specific requirements. For the fundamental investigations of heat transfer between a rolling sphere and plate, the solver has to fulfil several requirements that no standard solver incorporates, i.e. different regions for solids and fluids (gas or liquid), topological mesh movement, temperature dependent physical properties and arbitrary composition of the fluid phase. The postulated requirements can be met by modification of the standard solver *chtMultiRegionFoam* with:

- the *dynamicFvMesh* library for the topological mesh movement;
- a modified *thermophysicalModels* library for the temperature dependent properties;
- a link between energy and momentum balance, which describes the momentum dissipation.

The simulation domain is built with three different meshes, each representing a region with different physical properties, i.e. sphere, plate and surrounding gas phase. Fig. 1 shows the assembly.

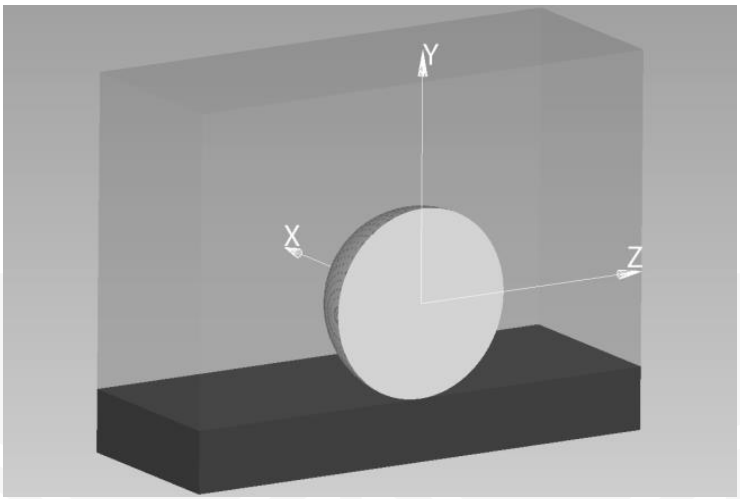

Fig. 1. CFD Domain with different regions: mid-grey – gas phase; dark grey – plate; light grey – sphere

2.2. Simulation conditions

For the fluid phase, the compressible Navier-Stokes equations

$$\frac{\partial \rho \hat{v}}{\partial t} + \nabla(\rho \hat{v}\hat{v}) = \nabla(\eta \nabla \hat{v}) - \nabla p + \rho g \tag{1}$$

are applied, although the Mach Number is small. The reason is to be able to implicitly link density and temperature with the perfect gas equation

$$pV = nRT. \tag{2}$$

The heat transfer is described with the energy equation

$$\frac{\partial \rho e + \frac{1}{2}\rho|\hat{v}|^2}{\partial t} + \nabla\left(\rho e + \frac{1}{2}\rho|\hat{v}|^2\right)\hat{v} = \nabla\left(\frac{\lambda}{c_p}\nabla e\right) - \nabla p\hat{v} + \rho g\hat{v} + \nabla\tau\hat{v} \tag{3}$$

incorporating convective and diffusive heat transfer terms as well as the dissipation term.

For the solid phase, the movement is described by a moving mesh approach and the diffusive heat transport is calculated with the equation for transient heat conduction

$$\frac{\partial \rho e}{\partial t} = \nabla\left(\frac{\lambda}{c_p}\nabla e\right). \tag{4}$$

The simulation is set up in a way, which implies the observer to be moving with the coordinate system at the same absolute velocity as the sphere does. This way the sphere's mesh only has to perform an according rotational movement within the surrounding gas

phase, whereas the translational movement is simulated by an approaching flow with according velocity. The plate is represented by a mesh adjacent to the bottom of the gas phase. Due to the prescribed view of a moving observer the plate has to perform a linear movement with the sphere's velocity. The plate's movement is represented by treating the plate as an inviscid fluid with the physical properties of a solid, so that the plate's mesh does not have to be moved. The mesh regions are coupled via a Cauchy boundary condition for the temperature and the temperature gradient respectively

$$T_{sphere,surface} = T_{fluid,surface} \tag{5}$$

$$\dot{q}_{sphere} = \dot{q}_{fluid} \tag{6}$$

By using the arbitrary mesh interface (AMI) mapping function, which works with an algorithm using Galerkin projection [5], the faces at the boundaries do not need to conform with adjacent faces.

During the evaluation of the equation system, different arithmetical operations have to be carried out including surface and volume integrals as well as time integration. In order to do this numerically, the operations have to be carried out in a discretised form. There are a variety of discretisation schemes available which have different influences on the solution of the equation system. The upwind differencing scheme increases solution stability due to numerically dissipative behaviour. This is a first-order scheme which means the interpolation error decreases linearly with an increasing discretisation resolution. On the other hand, higher order schemes, like central differencing schemes, behave in the opposite way. In Table 1, the applied discretisation schemes are listed for the gas region and the plate region. The significant difference lies in the scheme for the divergence discretisation. For the gas region, a scheme of high order, which is not diffusive, is applied in order to use the truncation error for turbulence creation. In contrast, a first order scheme, which is very diffusive, is applied for the plate region in order to supress any turbulence, since this region actually describes a solid.

Table 1

Spatial and temporal discretisation schemes for gas and plate region

region	temporal	gradient	divergence	Laplace
gas	Crank-Nicolson, 2^{nd} order	least squares, 2^{nd} order	central differencing, 4^{th} order	central differencing, 2^{nd} order
plate	Crank-Nicolson, 2^{nd} order	central differencing, 2^{nd} order	upwind, 1^{st} order	central differencing, 2^{nd} order

2.3. Meshing

As mentioned in section 2.1, the three different regions (i.e. sphere, gas and plate) are each treated with their own mesh. The meshes for the sphere and plate are physically describing solids where only the heat flux is investigated in this work. The resolution is

rather coarse compared to the gas region, so that the mesh generation is not described in detail. In the latter region, fluid dynamics is of high interest; therefore, the mesh generation is crucial. The mesh for direct numerical simulation in this region has to fulfil certain conditions. The spatial resolution has to be high in order to resolve all vortices down to where the energy is dissipated, the so-called *Kolmogorov* scale [6], which is basically determined by the viscosity.

$$\eta = \left(\frac{\nu^3}{\varepsilon}\right)^{1/4} \tag{7}$$

The mesh is built on the basis of a structured hexahedral mesh which is advantageous for parallelisation during the actual calculation. The sphere is inserted via the OpenFOAM® meshing tool *snappyHexMesh*. The grid is simultaneously refined in this step. Fig. 2 depicts the refined mesh assembly for all regions. The overall domain includes a very highly resolved region of interest, which was gained by previous turbulence modelling simulations. The point distance in each coordinate direction is maximal 25 µm wide. The surface of the sphere and the gap are resolved even with a smaller point distance. Employing the results from the DNS to equation (7) gives a *Kolmogorov* scale of about 50µm for this case, so that the condition is satisfied.

The contact point between the sphere and plate cannot be represented in a finite volume method. In the literature, several approaches can be found that introduce solutions for this task. The particle is flattened near to the contact point to leave a gap between two solid surfaces in the ‘caps’ approach by Eppinger et al. [7]. Dixon et al. [8], alternatively, give an overview of possible solutions; in particular, shrinking, overlap, bridge connection and an approach similar to the ‘caps’ approach.

Since this work is a fundamental investigation of heat transfer mechanisms, the characteristic geometry of the sphere should be conserved. The contact point is therefore replaced by a gap of 1µm width which is resolved with at least four finite volume cells.

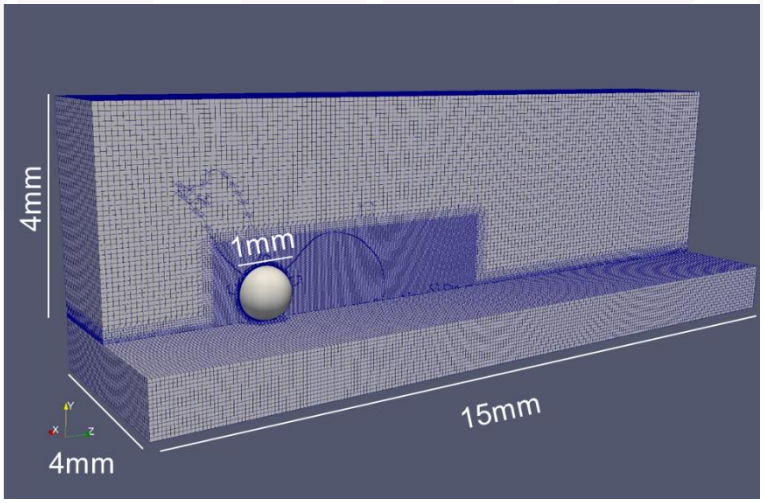

Fig. 2. Refined mesh assembly

2.4. Boundary conditions

The flow fields of the gas and plate are velocity driven since the pressure does not significantly change in this case. Constant values for velocity (5 m/s) and temperature (430 K) are applied at the inlet. At the outlet and the top of the gas phase region, a mixed boundary condition is applied – this changes between the Dirichlet and Neumann condition depending on the direction of the flux. Hereby, backflow into the domain, which might occur, can be handled. At the boundaries between gas and solid regions, the velocity is also fixed in order to represent the no slip condition for the mentioned moving observer. As mentioned in section 2.2, a Cauchy boundary condition for the temperature at the contact surfaces of the gas with the solid is implemented.

The velocity and pressure field results from the turbulence modelling simulations mentioned in section 2.3 were used as starting values for the direct numerical simulations in order to improve convergence. The initial values for the temperature were 550 K for the sphere and 430 K for the gas and plate region.

3. Results

Simulations with Reynolds Averaged Navier Stokes turbulence were carried out for the generation of starting values for the actual direct numerical simulation. In these steady state simulations, only the fluid dynamics in the gas phase was solved, neglecting the transient heat transfer. The OpenFOAM® standard solver *simpleFOAM* was used and both standard k-ε- and k-ω-SST-models were applied in a low-Reynolds approach with the absence of wall functions. Since the standard k-ε-model showed better stability in the convergence behaviour, the DNS was initialised with its results for velocity and pressure field.

The velocity magnitude field for both DNS and the standard k-ε-model are depicted in Fig. 3. One has to keep in mind that for an observer, who moves with the same velocity as the sphere does, the relative velocity is depicted. The domain's symmetry plane in rolling direction is shown, so that the sphere moves from right to left. For the transient DNS, a time-averaged velocity field is generated for comparison with the stationary RANS model. The simulations show qualitatively similar results with a slight difference in the description of the flow detachment. The direct numerical simulation predicts a more distinct vortex in the flow detachment area behind the sphere and a slightly different shape of the area near the wall.

In Fig. 4, the energy dissipation rate is shown for the same cases shown before. Both results show a qualitatively strong agreement. The highest values for the dissipation rate are predicted around the surface of the sphere and near to the plate in the sphere's wake. As can be seen in Fig. 3, there is a very sharp gradient near to the surface of the sphere due to its no slip condition. The displacement of fluid caused by the sphere enforces this effect by accelerating the fluid. Referring once more to the observer, who moves with the sphere's velocity, it can be seen, that downstream of the touching point of sphere and plate large gradients occur as well. The velocity gradients 'feed' eddies in which the energy is finally dissipated.

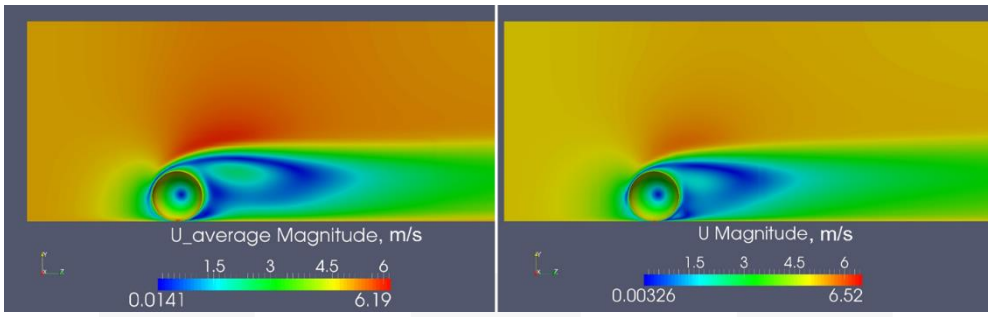

Fig. 3. Velocity magnitude fields: left – DNS; right – standard k-ε-model

Conversely, the quantity of the dissipated energy differs significantly. The DNS delivers much higher dissipation rates compared to the standard k-ε-model.

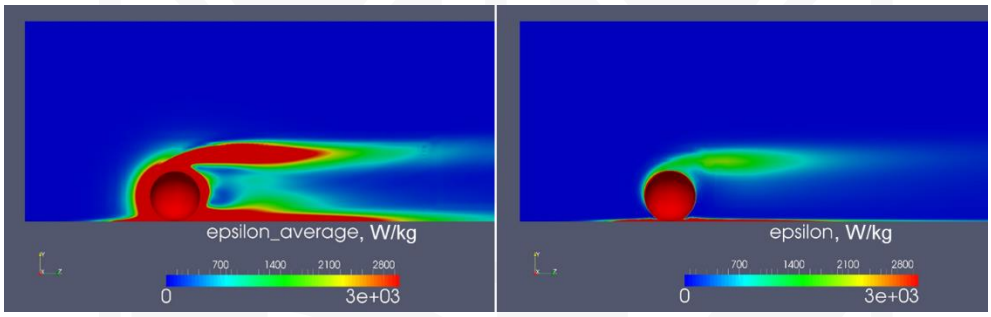

Fig. 4. Dissipation rate of turbulent kinetic energy: left – DNS; right – standard k-ε-model

In order to determine the influence of turbulence on the heat transfer, both convective and diffusive heat flux are calculated and shown in Fig. 5 for turbulent conditions (DNS, 5 m/s) on the left-hand side, and for a simulation under laminar conditions (0.1 m/s) on the right-hand side. In each picture, the convective heat flux is on the sphere's left-hand side and the diffusive heat flux on its right-hand side. The sphere rolls towards the observer, so that the fluid flow is in accord with the convective heat flux (Z-direction). Both vector fields are scaled in size with the absolute amount of heat flux. The heat flux component in the Y-direction (i.e. normal to the plate) is represented in colour. Due to the no slip condition on the sphere's surface, heat is convectively transported to the plate on the sphere's front side and transported away on the rear side. On the other side, heat is diffusively transported by conduction in normal direction to the plate. In the turbulent case, both mechanisms take place at the same order of magnitude, whereas in the laminar case, the diffusive transport clearly dominates. In Table 2, the overall heat transfer coefficients for the wall-heat transfer

$$k_{sphere/wall} = \frac{\dot{Q}_{projection}}{A_{projection}(\bar{T}_{projection} - \bar{T}_{lower\ hemisphere})} \tag{8}$$

and the heat transfer towards the surrounding fluid

$$k_{sphere/gas} = \frac{\dot{Q}_{sphere}}{A_{sphere}(\bar{T}_{sphere} - \bar{T}_{gas})} \tag{9}$$

are listed. For $k_{\text{sphere/wall}}$, the overall heat flux into the plate is integrated over the sphere's projection area and area averaged values are applied for the temperature difference. For $k_{\text{sphere/gas}}$, the heat overall flux into the gas phase is integrated over the surface of the sphere and again area averaged values are applied for the temperature difference.

The wall-heat transfer is not significantly affected by the occurrence of turbulence, whereas the heat transfer towards the surrounding fluid increases.

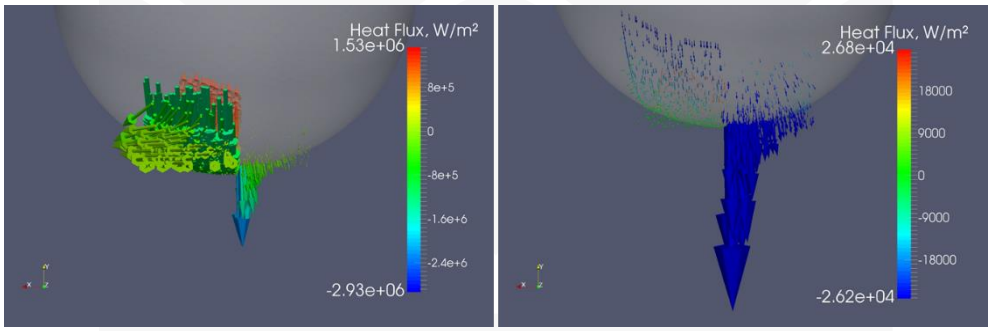

Fig. 5. Convective and diffusive heat flux: left – DNS; right – laminar

Table 2

Overall heat transfer coefficients

regime	$k_{\text{sphere/wall}}$, W/m²K	$k_{\text{sphere/gas}}$, W/m²K
turbulent	790	437
laminar	807	317

4. Summary & Conclusion

In this paper, a first direct numerical simulation of a rolling sphere on a flat plate incorporating heat transfer is shown. The fluid dynamics is compared against a stationary RANS simulation with the standard k-ε-model. It is shown that the turbulence model underestimates the dissipation of turbulent kinetic energy in comparison to the solution of the DNS.

In the second step, the result for the heat transfer is compared against a simulation of the heat transfer under laminar conditions. Although the convective heat flux is shown to have

increased with the presence of turbulence, the overall wall-heat transfer coefficient does not change significantly from the laminar to the turbulent regime. Nevertheless, the heat transfer from the sphere to the surrounding gas phase increases with rolling speed and occurring turbulence as expected due to the decreased thickness of the boundary layer.

5. Outlook

The thesis that the presence of turbulence seems to have negligible influence on the heat transfer between a rolling sphere and a plate has to be verified by a wider range of parameter variation (e.g. velocity, diameter). To this aim, further simulations with turbulence models are planned. It has to be established if the standard k-ε-model's parameters can be calibrated with the result from the DNS in order to represent the correct velocity field and amount of dissipated energy.

References

[1] Brösigke G., Herter A., Rädle M., Repke J.-U., *Investigations of Heat Transfer Mechanisms between a Moving Sphere and a Static Plate with Computational Fluid Dynamics*, 17th Conference on Process Integration, Modelling and Optimisation for Energy Saving and Pollution Reduction, Prague 24.-27.8.2014.

[2] Schlünder E.-U., Chem. Eng. Process., vol. 18, 1984, 31-53.

[3] Weller H.G., Tabor G., Jasak H., Fureby C., *A tensorial approach to computational continuum mechanics using object-oriented techniques*, Computers In Physics, vol. 12(6) 1998, DOI: 10.1063/1.168744.

[4] Jasak H., *Error analysis and estimation for the finite volume method with applications to fluid flows*, PhD Imperial College London (University of London) 1996.

[5] Farrell P.E; Maddison J.R, *Conservative interpolation between volume meshes by local Galerkin projection*, Computer Methods In Applied Mechanics And Engineering vol. 200(1-4), 2011, 89-100, DOI: 10.1016/j.cma.2010.07.015.

[6] Ferziger J.H., Perić M., *Computational Methods for Fluid Dynamics*, Springer, Berlin, Heidelberg 2002.

[7] Eppinger T.; Seidler K.; Kraume M., *DEM-CFD simulations of fixed bed reactors with small tube to particle diameter ratios*, Chemical Engineering Journal, vol. 166(1), 2011, 324-331, DOI: 10.1016/j.cej.2010.10.053.

[8] Dixon A.G.; Nijemeisland M., Stitt E.H., *Systematic mesh development for 3D CFD simulation of fixed beds: Contact points study*, Computers & Chemical Engineering vol. 48, 2013, 135-153, DOI: 10.1016/j.compchemeng.2012.08.011.